Electronic Supplementary Material (ESI) for Physical Chemistry Chemical Physics.

Supporting Information

UV absorption probing of the conformer-dependent reactivity of a Criegee intermediate CH_3CHOO

Leonid Sheps, Ashley M. Scully, and Kendrew Au*

Transient absorption measurements

The experimental apparatus is a slow-flow chemical reactor integrated into a cavity-enhanced absorption spectrometer, operating in the UV-VIS spectral range. Full details of the setup have been recently published,[1] so only a summary is given here. A schematic of the apparatus is shown in Fig. S1.

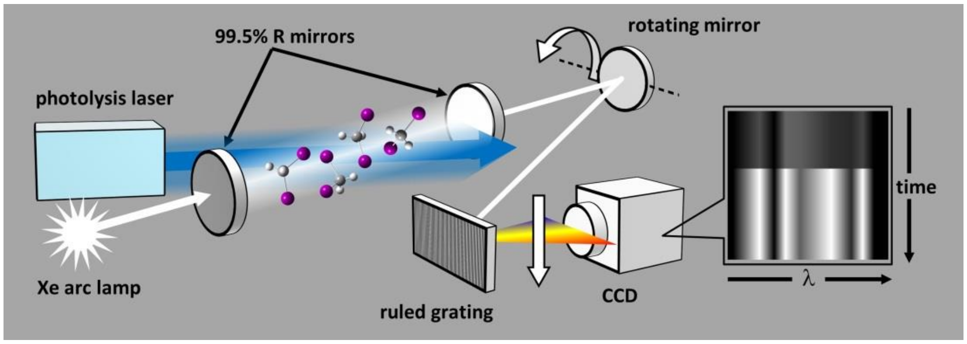

Fig. S1. Schematic of the Time-Resolved Broadband Cavity-Enhanced Absorption Spectrometer.

The reactor is a 1.6 m-long quartz cell, pumped by a roots pump and kept at a constant pressure using a PID-controlled butterfly valve to throttle the pumping speed. The sample mixture consists of small amounts of CH_3CHI_2, O_2(99.9999%), SO_2(0.286% diluted in He), H_2O, and He buffer gas (99.9999%). The liquid reagents (CH_3CHI_2 and H_2O) are delivered by entraining their vapor in He using glass bubblers kept at a constant temperature of 20°C. The desired concentrations of CH_3CHI_2 and H_2O in the reactor are obtained by adjusting the total pressure in their respective bubblers and thus their dilution factor in the He entrainment flow. Individual flows of the sample mixture components are regulated by calibrated mass flow controllers and are mixed at the entrance to the reactor. All data were taken at $T = 293$ K.

The multipass optical resonator (cavity) is incorporated directly into the reactor volume. A Xe arc lamp provides continuous broadband probe radiation that spans the 200 – 2000 nm range, and a BG-3 optical filter attenuates the wavelengths outside of the 300 – 450 nm range of interest for the present study. The effective path length (L_{eff}) inside the cavity is measured independently with known absorption cross-sections of NO_2 and CH_2I_2.[2,3] In the current experiments L_{eff} varies between 50 and 70 cavity passes, depending on the wavelength, because of the slight variations in reflectivity of the broadband cavity mirrors. The reaction of CH_3CHI with O_2 is initiated by photodissociation of the CH_3CHI_2 precursor using a 266-nm laser pulse from the 4th harmonic of a YAG laser. The photolysis laser path and the optical cavity axis intersect at a 2° angle and overlap over a path length $L = 80$ cm, for a total absorption path length $L_{eff} = 40 – 56$ m.

The transient absorption measurements are acquired by a custom-built spectrometer. The continuous cavity output is dispersed in wavelength horizontally by a ruled grating and focused onto a 1024x1024 pixel CCD camera. A precisely controlled phase-locked spinning mirror in the light path sweeps the entire probe spectrum vertically over the CCD detector, such that the spectral and temporal information are mapped spatially along the *x* and *y* dimensions, respectively, of the CCD sensor. The timing of the photolysis laser is synchronized with the spinning mirror and therefore with the probe radiation sweep. The transient absorption is integrated directly on the CCD detector for many laser shots with the camera shutter open, and read out at the end of a “long exposure” mode, bypassing the need for fast data transfer equipment.

Our wavelength scale (resolution ~1.5 nm FWHM) is calibrated using atomic emission lines from a Hg(Ne) pencil lamp; kinetic time scale (resolution ~50 μs FWHM) is calibrated by varying the photolysis laser delay. Transient absorption is calculated using the difference between "photolysis ON" and "photolysis OFF" images. For the experiments described here, we average between 100 and 5400 laser shots for each experimental condition. The absorbance, expressed in units of optical density, is calculated according to the Beer-Lambert equation:

$$OD = -ln(I/I_0) = C \cdot \sigma_{abs} \cdot L_{eff} \tag{1}$$

Here I and I_0 are the probe radiation intensity with and without the photolysis laser, respectively, C is the transient absorber concentration, σ_{abs} is the absorption cross-section, and L_{eff} is the effective optical path length in the reactor cavity. All transient images shown here have been smoothed with a 5-pixel Gaussian filter, which does not affect the stated experimental resolution.

Identification of long-lived transient absorption bands

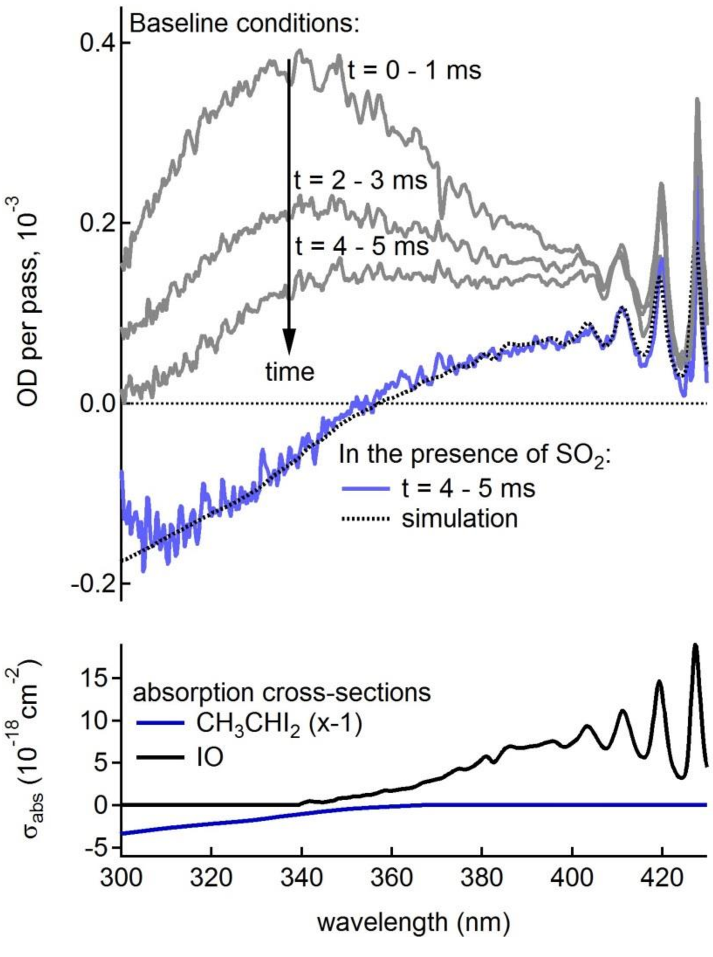

Fig. S2. *Upper panel:* Select transient spectra of the reaction $CH_3CHI + O_2$. Spectra shown in gray were taken at baseline condition (only O_2 and CH_3CHI_2 in He bath), averaged over kinetic times t = 0 – 1, 2 – 3, and 4 – 5 ms. The spectrum in blue was averaged over t = 4 – 5 ms in the presence of $4.7 \cdot 10^{13}$ cm^{-3} SO_2. Dotted black line is a spectral simulation that includes the formation of $1.2 \cdot 10^{11}$ cm^{-3} of IO and depletion of $7 \cdot 10^{11}$ cm^{-3} of CH_3CHI_2. *Lower panel:* literature absorption cross-sections of IO[4] and CH_3CHI_2.[5] The diiodoethane spectrum has been inverted to represent depletion by laser photolysis.

Figure S2 shows transient absorption spectra at several experimental conditions, averaged over different kinetic times after the photolysis pulse. The spectra shown in gray were averaged over different kinetic times at baseline conditions, meaning that the only species present before photolysis were the radical precursor ($[CH_3CHI_2] = 1.5\cdot10^{13}$ cm^{-3}) and oxygen ($[O_2] = 1.65\cdot10^{16}$ cm^{-3}) in He buffer gas at P = 10 torr. The spectra contain several overlapping absorption signals, including an intense broad band centered at ~340 nm and a structured absorption feature at longer wavelengths. The spectrum plotted in blue was taken in the presence of SO_2 (an efficient Criegee intermediate scavenger[6]), averaged over late kinetic times t = 4 – 5 ms, such that CH_3CHOO would react away and could no longer contribute to the transient absorption. This spectrum shows that the broad 340-nm band has decayed; the remaining long-lived absorption signals consist of the formation of IO and the photolytic depletion of CH_3CHI_2 which can be quantified using their known cross-sections.[4,5] A spectral simulation (dotted black line in Fig. S2) shows the formation of ~$1.2\cdot10^{11}$ cm^{-3} IO and depletion ~$7\cdot10^{11}$ cm^{-3} of CH_3CHI_2. This depletion corresponds to photodissociation of ~4.7% of the initial CH_3CHI_2 concentration, which is in excellent agreement with the expected value of 4.6% depletion based on the photolysis laser fluence.

The blue spectrum in Fig. S2 also reveals a weak unidentified absorption feature, which is responsible for the discrepancy between the experimental data and the simulation at wavelengths $\lambda < 310$ nm. This absorption signal appears promptly after photolysis and does not vary with kinetic time; therefore, it does not influence the results and conclusions of this study. The unidentified spectral band, along with transient signals due to IO formation and precursor depletion are quantified and then subtracted from each dataset at various experimental conditions in order to focus on the absorption spectrum of CH_3CHOO.

Subtraction of background signals

All background signals other than the absorption of CH_3CHOO were subtracted from the total transient absorption images in a procedure outlined previously,[7] by quantifying the positive (formation) signal due to IO and the negative (depletion) signal die to photolysis of CH_3CHI_2.

IO formation. The IO signal was quantified by its transient absorption at 427 nm, as shown in Fig. S3 for a representative trace in the presence of $1\cdot10^{11}$ cm^{-3} of H_2O. The IO kinetic trace was fit to a sum of two rising exponential functions, convoluted with experimental time resolution. The prompt signal rise in this

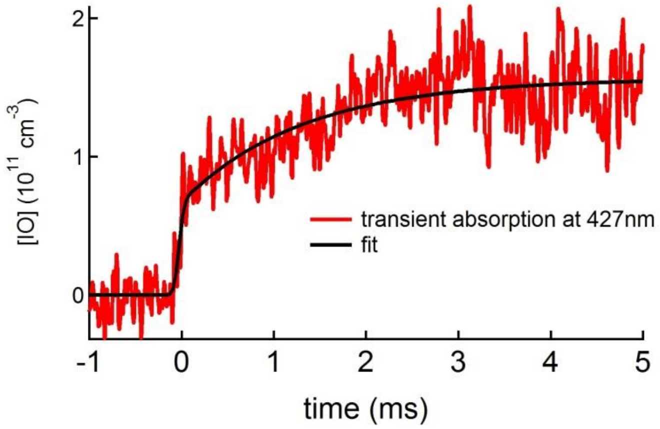

Fig. S3. Quantification of IO formation in the reaction $CH_3CHI + O_2$ in the presence of $1\cdot10^{11}$ cm^{-3} of H_2O. Red line: IO concentration determined from the transient absorption at $\lambda = 427$ nm; black line: kinetic fit to a sum of two rising exponential functions, convoluted by experimental time resolution.

example accounts for (6.5±1)·10^{11} cm^{-3} of IO formed directly by $CH_3CHI + O_2$ or by other fast reactions, whereas the slow rise accounts for (9±1)·10^{11} cm^{-3} of IO formed by secondary chemistry. The errors in the IO concentrations reflect the uncertainty of the fit and of the published IO absorption cross-sections.

CH_3CHI_2 depletion. The initial concentration of CH_3CHI_2 in all experiments reported here was $1.51\cdot10^{13}$ cm^{-3}; its absorption cross-section[5] at 266 nm is ~$1.45\cdot10^{-18}$ cm^2. The photolysis laser fluence was maintained (typically 24 mJ/cm^2) to ensure approximately 5% dissociation of CH_3CHI_2. The absolute number density of photodissociated CH_3CHI_2 was quantified at long kinetic times in the presence of SO_2 (see above), and agreed very well with calculated values. Laser photolysis is essentially instantaneous on our experimental timescales, so the temporal evolution of the precursor depletion was modeled by a step function, convoluted with our time resolution.

Deconvolution of *syn*- and *anti*-CH_3CHOO absorption spectra

The transient absorption image in the presence of high water concentration ([H_2O] = $1\cdot10^{17}$ cm^{-3}) reveals that the intense spectral band at ~340 nm appears to decay quickly on its low-energy side and slowly on the high-energy side, suggesting two separate components. The two spectral contributions to the total transient absorption of CH_3CHOO were separated by integration over different kinetic times and further confirmed by kinetic fitting at different probe wavelengths.

Determination of appropriate kinetic fit function. All kinetic measurements described in this manuscript were performed under pseudo-1st-order conditions. In order to assure that our experimental signals had minimal interference from radical-radical reactions, we investigated possible contributions to our kinetic fit functions from 2nd-order kinetics.

For reaction R2, the O_2 concentration was sufficiently high to ensure signal rise times of 2000 – 12000 s^{-1}. If the self-reaction CH_3CHI radicals is similar to that of CH_2I (k_{self} ~$4\cdot10^{-11}$ $cm^6\cdot molecule^{-2}\cdot s^{-1}$)[8], this self-reaction has apparent 1st-order rate of ~50 s^{-1} at our experimental conditions. Such a small contribution does not noticeably affect the fits and therefore has a negligible impact on the measured kinetics of reaction $CH_3CHI + O_2$.

Similarly, reactions R3 ($CH_3CHOO + SO_2$) and R4 ($CH_3CHOO + H_2O$) could have contributions from the self-reaction of acetaldehyde oxide. If we assume a self-reaction rate that is independent of conformer and similarly fast to the case of CH_2OO[9,10] (~$6\cdot10^{-11}$ $cm^6\cdot molecule^{-2}\cdot s^{-1}$), the apparent 1st-order decay of CH_3CHOO due to self-reaction is ~60 s^{-1} at our initial radical concentrations. Incorporating self-reaction into our kinetic fits did not significantly improve the fit quality, and therefore a determination of the self-reaction rate coefficient was not feasible purely from the kinetic fits. Including the self-reaction rate at the fixed value for CH_2OO by Ting *et al.*[10] decreased all first-order decay rates by ~60 s^{-1}, but did not affect the second order rate coefficients k_3 and k_4 at all.

Therefore, our system is described well by 1st-order kinetics, and we used fit functions made up of simple exponential rise and decay components in our measurements of reaction kinetics.

Kinetic fitting procedure. Figure 2 in the main text shows the transient absorption in the presence of $1\cdot10^{11}$ cm^{-3} of H_2O averaged over λ = 320 – 400 nm after subtraction of background signals. The time evolution of the absorption signal is fit to a sum of two independent components:

$$S_{tot}(t) = S_{syn}(t) + S_{anti}(t) \tag{1}$$

Each component has single exponential rise and decay, as an intermediate (B) in a simple sequential kinetics scheme, $A \overset{k_a}{\rightarrow} B \overset{k_b}{\rightarrow} C$:

$$S_i(t) = \frac{A_i \cdot k'_{a,i}}{k'_{a,i} - k'_{b,i}} [e^{-k'_{b,i} \cdot t} - e^{-k'_{a,i} \cdot t}] \tag{2}$$

Here *S(t)* is the experimental time-resolved signal, k'_a and k'_b are the first-order rise and decay rates, and A is the amplitude. Since *syn*- and *anti*-CH_3CHOO are formed together by reaction R2, the rise times of both components were fixed at 132,000 s^{-1}, which corresponds to the pseudo-first order rate of reaction $CH_3CHI + O_2$ at current conditions. The other parameters for the two components were allowed to vary, and the decay rates of the fast and slow component were 2800±300 s^{-1} and 175±25 s^{-1}, respectively. We attempted to vary the fitting routine, such as allowing all coefficients to vary or including an additional long-time offset to compensate for imperfect background subtraction. However, such adjustments did not improve the fit quality greatly. The reported errors in the decay rates include fit uncertainties, systematic errors due to the choice of the fitting procedure, and variability of fits to data collected on different days.

The large difference of the two decay timescales allowed a clean separation of the absorption spectra of the two fit components. Averaging the transient absorption over times t = 1 – 2 ms yields the spectrum of only the slow component, *syn*-CH_3CHOO. Subtracting this spectrum (appropriately scaled) from the total absorption spectrum provides the difference spectrum due to the fast component, *anti*-CH_3CHOO. The intensities of the spectra reported in Fig. 2 of the main text are extrapolated back to time t = 0 using the amplitudes A_{syn} and A_{anti} from the kinetic fit.

Kinetic fits at different probe wavelengths. In order to strengthen our conclusion we performed additional analysis by fitting transient absorption time traces averaged over six different 20 nm-wide spectral slices, centered at 310, 330, 350, 370, 390, and 410 nm. The six separate kinetic traces were fit

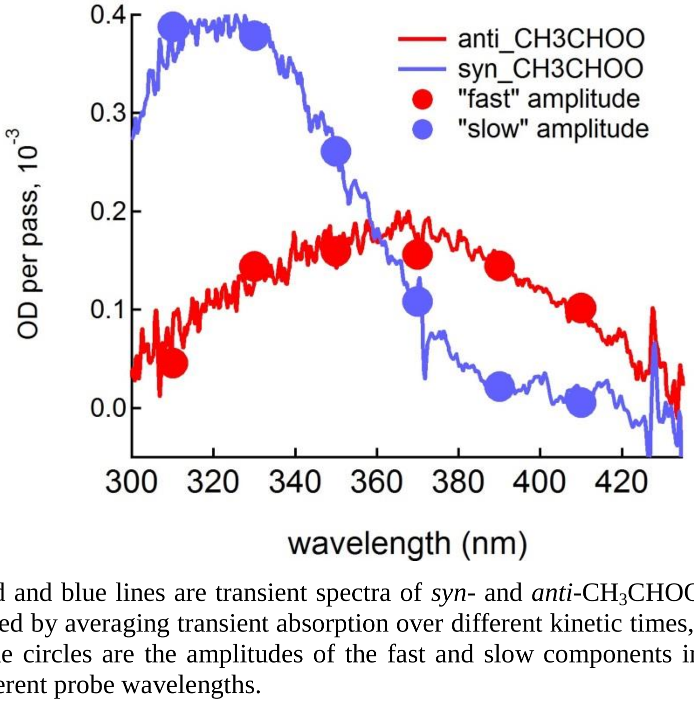

Fig. S4. Solid red and blue lines are transient spectra of *syn*- and *anti*-CH_3CHOO (extrapolated to kinetic time t = 0) obtained by averaging transient absorption over different kinetic times, as described in the main text. Red and blue circles are the amplitudes of the fast and slow components in kinetic fits of transient absorption at different probe wavelengths.

simultaneously, and the rise times were again fixed at 132,000 s^{-1}. The decay rates of the fast and slow components were constrained to be the same at all wavelengths and yielded values of 2870 s^{-1} and 195 s^{-1}, within the uncertainty limits stated above. The amplitudes were allowed to vary as a function of wavelength, and the results are shown in Fig. S4. These amplitudes agree very well with the transient spectra of *syn*- and *anti*-CH_3CHOO obtained by averaging over early and late kinetic times, extrapolated to t = 0 (also included in Fig. S4). The agreement of both, signal amplitudes *and* decay rates, obtained by two complementary approaches demonstrates that our analysis is self-consistent and bolsters our main conclusion that the intense transient absorption feature in the 340-nm region is dominated by two spectral bands with decay times that differ by a factor of 16 (~2800 and ~175 s^{-1}).

Kinetics of the $CH_3CHI + O_2$ reaction

The rate coefficient for the reaction $CH_3CHI + O_2$ is obtained from kinetic fits of the transient absorption at varying [O_2] without adding SO_2 or H_2O. In principle, two kinetic components are needed to describe the time evolution of *syn*- and *anti*-CH_3CHOO. However, we found that in practice a one-component fit was sufficient to fit the experimental traces very well, and adding a second component did not improve the fit. Instead, one of the two components typically converged to non-physical values, which shows that the second component was not needed. This means that the rise and decay times of both CH_3CHOO conformers are quite similar in the absence of any Criegee intermediate scavengers, and the system can be described by a simplified kinetic scheme:

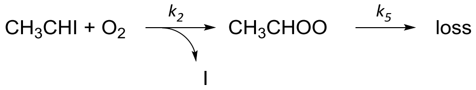

The time-resolved signals are therefore fit to a single exponential rise and decay with functional form as in Eq. (2).

$$S(t) = \frac{A\cdot k_2'}{k_2'-k_5}\left[e^{-k_5\cdot t} - e^{-k_2'\cdot t}\right] \qquad (3)$$

Here k_2' is the pseudo-first order rate of formation of CH_3CHOO, $k_2' = k_2\cdot[O_2] + k_2^0$. The quantity k_2 is the bimolecular rate coefficient of reaction R2, and k_2^0 is the first-order loss term that includes the removal of the initial CH_3CHI radical by all other processes. k_5 (the sum of first order losses of CH_3CHOO) governs the decay of the transient absorption, whereas its rise time is determined by k_2'. A plot of k_2' as a function of [O_2] allows the determination of k_2.

Two sets of data fitting were performed. In the first, we fit the time evolution of the transient absorption averaged over λ = 320 – 400 nm. In the second, we fit separately the absorption traces averaged over five different 20-nm wide spectral slices, centered at 330, 350, 370, 390, and 410 nm. The traces at shorter wavelengths are dominated by Band I; those at longer wavelength are dominated by Band II. Figure S5 compares the results obtained by these two approaches. The transient absorption rise times do not depend on the probe wavelengths, which validates our initial assumption that both *syn*- and *anti*-CH_3CHOO are formed with the same rate.

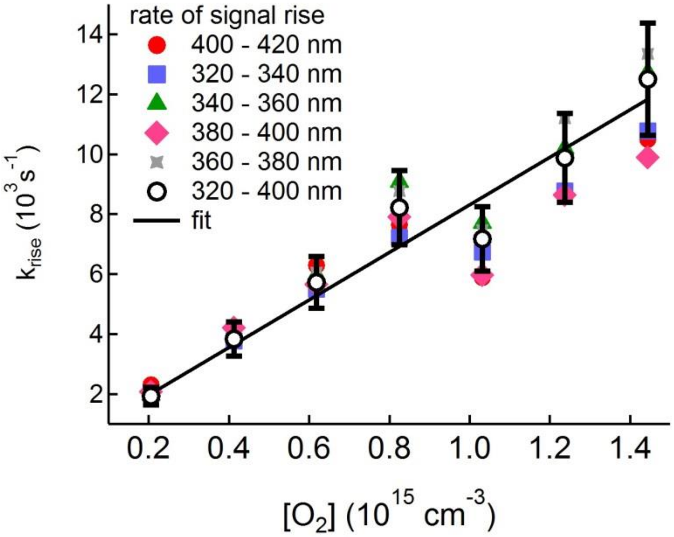

Fig. S5. Comparison of the fitted values of $\boldsymbol{k_2'}$ (the inverse of the signal rise time at varying [O_2]), using absorption traces averaged over different spectral ranges.

Comparison with UV spectrum of CH_3CHOO by Smith *et al.*[11]

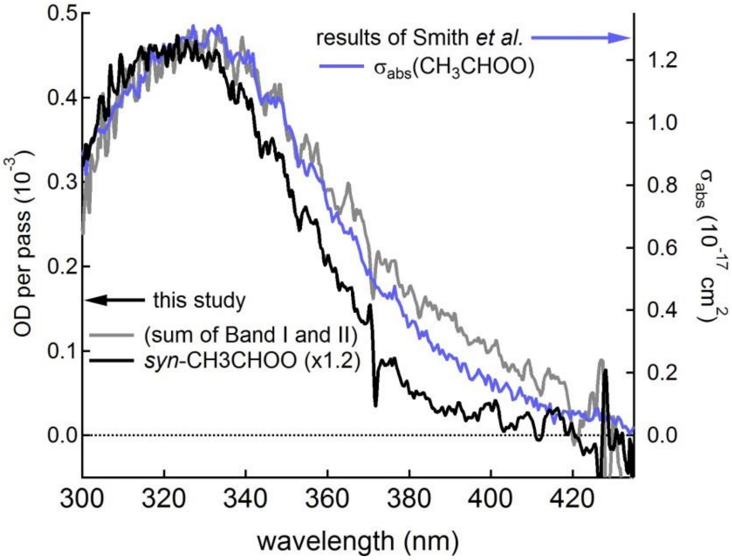

Fig. S6. Comparison of the UV spectra in this study with the absolute absorption spectrum of CH_3CHOO by Smith *et al.* The gray and black spectra are plotted such that their maximum intensities match that of the Smith *et al.* spectrum.

We compared the UV spectra of CH_3CHOO from our experiments with the published results of Lin and co-workers. When scaled such that their maximum intensities match (shown in Fig. S6), the spectrum of Smith *et al.* resembles the total transient absorption (sum of Band I and Band II) in this study, although our signal to noise ratio is somewhat worse. The spectrum of the *syn*-confomer (Band I) is slightly blue-shifted relative to that of Smith *et al.* and is less intense on the long-wavelength side; the *anti*-CH_3CHOO spectrum (Band II) is substantially red-shifted from Band I.

Calculation of solar photolysis lifetimes of *anti*-CH_3CHOO

The photolysis lifetime of *anti*-CH_3CHOO was calculated following the method of Smith *et al.*,[11] as the inverse of the *J*-value (the first-order rate of photolysis), which is calculated using the equation

$$J = \int_{\lambda_1}^{\lambda_2} \sigma(\lambda)\Phi(\lambda)F(\lambda)d\lambda \tag{4}$$

Here $\sigma(\lambda)$ is the absorption cross-section, $\Phi(\lambda)$ is the photolysis yield (assumed to be unity at all wavelengths), and $F(\lambda)$ is the solar actinic flux. The values of $F(\lambda)$ were obtained from the NCAR Tropospheric Ultraviolet and Visible (TUV) calculator (http://cprm.acd.ucar.edu/Models/TUV/), similar to Smith *et al.* The calculation was performed for conditions at the Earth's surface using three different solar zenith angles (SZA), as shown in Fig. S7. The photolysis rate *J*, integrated over the absorption band of *anti*-CH_3CHOO from λ = 300 – 435 nm, is 0.26 s^{-1}, 0.24 s^{-1}, and 0.15 s^{-1} for SZA of 0, 30, and 60°, respectively. The corresponding solar lifetimes are 3.8 s, 4.1 s, and 6.6 s.

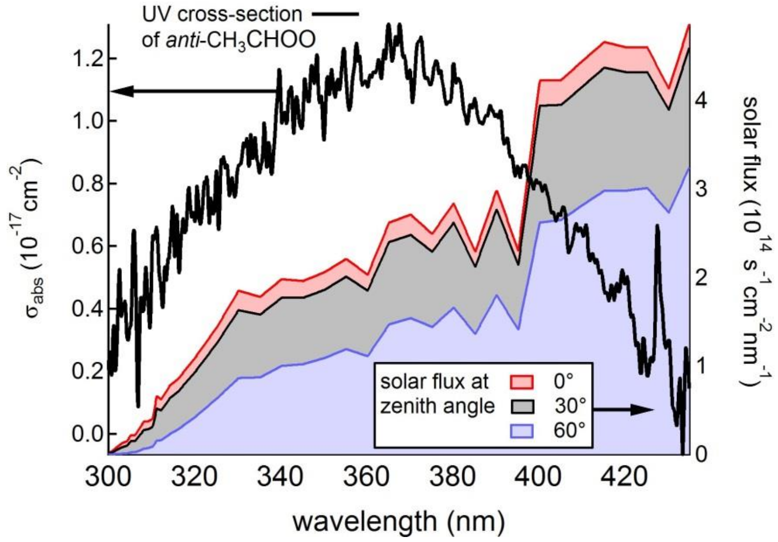

Fig. S7. UV absorption cross-section of CH_3CHOO (black line) and estimated solar actinic flux at the Earth's surface at solar zenith angles of 0, 30, and 60°.

1. L. Sheps and D. W. Chandler, *Time-resolved broadband cavity-enhanced absorption spectrometry for chemical kinetics* SAND2013-2664, Sandia National Laboratories, Livermore, CA, 2013.
2. K. Bogumil, J. Orphal, T. Homann, S. Voigt, P. Spietz, O. C. Fleischmann, A. Vogel, M. Hartmann, H. Kromminga, H. Bovensmann, J. Frerick and J. P. Burrows, *J. Photochem. Photobiol., A*, 2003, **157**, 167-184.
3. S. Sander, R. Friedl, J. Barker, D. Golden, M. Kurylo, P. Wine, J. Abbatt, J. Burkholder, C. Kolb and G. Moortgat, *Chemical Kinetics and Photochemical Data for use in Atmospheric Studies–Evaluation* JPL Publication 10–6, Jet Propulsion Laboratory, Pasadena, CA.
4. M. H. Harwood, J. B. Burkholder, M. Hunter, R. W. Fox and A. R. Ravishankara, *J. Phys. Chem. A*, 1997, **101**, 853-863.
5. G. Schmitt and F. Comes, *Journal of Photochemistry*, 1980, **14**, 107-123.
6. O. Welz, J. D. Savee, D. L. Osborn, S. S. Vasu, C. J. Percival, D. E. Shallcross and C. A. Taatjes, *Science*, 2012, **335**, 204-207.
7. L. Sheps, *The Journal of Physical Chemistry Letters*, 2013, **4**, 4201-4205.
8. J. Sehested, T. Ellermann and O. J. Nielsen, *Int. J. Chem. Kinet.*, 1994, **26**, 259-272.
9. Z. J. Buras, R. M. Elsamra and W. H. Green, *The Journal of Physical Chemistry Letters*, 2014, **5**, 2224-2228.
10. W.-L. Ting, C.-H. Chang, Y.-F. Lee, H. Matsui, Y.-P. Lee and J. J.-M. Lin, *The Journal of chemical physics*, 2014, **141**, 104308.
11. M. C. Smith, W.-L. Ting, C.-H. Chang, K. Takahashi, K. A. Boering and J. J.-M. Lin, *The Journal of chemical physics*, 2014, **141**, 074302.